

Interplay of quantum spin Hall effect and spontaneous time-reversal symmetry breaking in electron-hole bilayers. I. Transport properties

Tania Paul ¹, V. Fernández Becerra,¹ and Timo Hyart ^{1,2,3}

¹*International Research Centre MagTop, Institute of Physics, Polish Academy of Sciences, Aleja Lotników 32/46, PL-02668 Warsaw, Poland*

²*Department of Applied Physics, Aalto University, 00076 Aalto, Espoo, Finland*

³*Computational Physics Laboratory, Physics Unit, Faculty of Engineering and Natural Sciences, Tampere University, FI-33014 Tampere, Finland*

 (Received 3 June 2022; revised 15 November 2022; accepted 13 December 2022; published 20 December 2022)

The band-inverted electron-hole bilayers, such as InAs/GaSb, are an interesting playground for the interplay of quantum spin Hall effect and correlation effects because of the small density of electrons and holes and the relatively small hybridization between the electron and hole bands. It has been proposed that Coulomb interactions lead to a time-reversal symmetry broken phase when the electron and hole densities are tuned from the trivial to the quantum spin Hall insulator regime. We show that the transport properties of the system in the time-reversal symmetry broken phase are consistent with recent experimental observations in InAs/GaSb. Moreover, we carry out a quantum transport study on a Corbino disk where the bulk and edge contributions to the conductance can be separated. We show that the edge becomes smoothly conducting and the bulk is always insulating when one tunes the system from the trivial to the quantum spin Hall insulator phase, providing unambiguous transport signatures of the time-reversal symmetry broken phase.

DOI: [10.1103/PhysRevB.106.235420](https://doi.org/10.1103/PhysRevB.106.235420)

I. INTRODUCTION

The advent of topological materials [1,2] has brought band-inverted semiconductors, with small electron and hole densities, to the focus of attention in the search for quantum spin Hall (QSH) insulators [3–8]. However, the electron-electron interactions are important in these materials if the hybridization of the electron and hole bands is small compared to the exciton binding energy, as can be appreciated by noting that the bilayer system of spatially separated electrons and holes is the well-known paradigm system for the realization of an exciton condensate state [9,10]. Indeed, it is now theoretically understood that interactions can lead to a plethora of correlated phases in band-inverted semiconductors [11–17] and recent experiments have shown evidence of excitonic phenomenology in InAs/GaSb quantum wells [18–22] as well as in WTe₂ [23,24]. We concentrate on the correlated phases appearing in the band-inverted electron-hole bilayers shown in Fig. 1(a) [4]. In these systems, the electron and hole bands are spatially separated and therefore only weakly hybridized. Moreover, the electron and hole densities (and hence also the band-inversion parameter E_G) can be controlled *in situ* with front and back gate voltages, V_f and V_b , allowing the possibility to study the phase transition between trivial and QSH insulator phases [4,22,25], as schematically illustrated in Fig. 1(b). It has been theoretically predicted that, due to the excitonic correlations caused by the Coulomb interactions, a third phase with spontaneously broken time-reversal symmetry (TRS) will appear in the transition regime between the

two topologically distinct phases [11]. Within this phase, the helical edge states, originating from the QSH insulator phase, can exist but they are not protected against backscattering, and it was theoretically demonstrated [11] that these unprotected edge states can explain the temperature-independent mean-free path observed in InAs/GaSb bilayers in the presence of reasonably large applied currents [7,26,27]. However, an unambiguous experimental demonstration of the existence of the exotic insulating phase with spontaneously broken TRS symmetry is still lacking in these systems.

Here we demonstrate that the transport properties of the system in the TRS broken phase are also consistent with more recent transport experiments in InAs/GaSb bilayers with small applied currents [28], so the spontaneous TRS symmetry breaking provides a comprehensive explanation of the temperature, voltage, and length dependencies of the observed conductance [7,26–28]. Finally, we propose an experiment which can be used to unambiguously demonstrate the existence of the spontaneous TRS breaking in this system, namely, we show that the edge becomes smoothly conducting and the bulk remains insulating when one tunes across the TRS broken phase appearing between the trivial and QSH insulator phases in the Corbino geometry, where the bulk and edge contributions to the conductance can be separated [29]. In the presence of TRS symmetry, the bulk transport gap must close when the system is tuned between topologically distinct phases, and hence the experimental demonstration of a transition without a bulk transport gap closing constitutes a proof of an existence of TRS broken insulating phase.

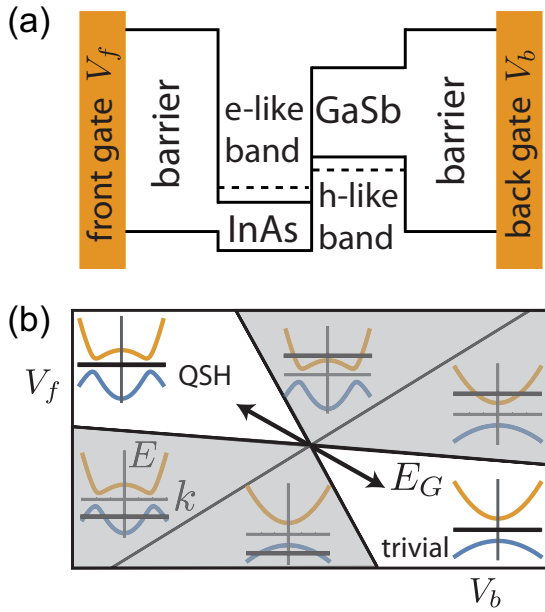


FIG. 1. Schematic illustration of the setup. (a) The densities of the electrons and holes can be controlled with gate voltages V_f and V_b in a heterostructure supporting spatially separated electron and hole bands. (b) This way, the gate voltages determine whether the electron and hole bands are inverted at the Γ point ($E_G > 0$) or not ($E_G < 0$), as well as whether the Fermi level (thick black line) is in the conduction band, band gap, or valence band. The insulating phase with $E_G > 0$ ($E_G < 0$) is the QSH (trivial) insulator phase.

II. SPONTANEOUS TRS BREAKING IN ELECTRON-HOLE BILAYERS

In Ref. [11], it was shown using a full Hartree-Fock calculation that the Coulomb interactions in the Bernevig-Hughes-Zhang (BHZ) model [3] developed for InAs/GaSb bilayers [4,30] lead to three different phases as a function of the hybridization of the electron and hole bands A and the band-inversion parameter E_G , which is defined here so for $E_G > 0$ ($E_G < 0$) the electron and hole bands are (not) inverted at the Γ point, see Fig. 1(b). As intuitively expected, for small (large) A and E_G one realizes a trivial (QSH) insulator phase. However, interestingly, it was found that at intermediate values of A and E_G there exists an insulating phase with spontaneously broken TRS symmetry separating the topologically distinct phases. In this section, we describe a simplified *minimal model* that fully captures all the essential results obtained using the full Hartree-Fock calculations in Ref. [11].

The single particle BHZ Hamiltonian is

$$H_0 = \left(\frac{\hbar^2 k^2}{2m} - E_G \right) \tau_z \sigma_0 + Ak_x \tau_x \sigma_z - Ak_y \tau_y \sigma_0 + \Delta_z \tau_y \sigma_y, \quad (1)$$

where τ 's and σ 's denote the Pauli matrices in the electron-hole and spin basis, respectively. The electron band is made out of s orbitals and the hole band is made out of only two p orbitals because the electric confining potential and the atomic spin-orbit coupling remove the degeneracies of the

p orbitals. The tunneling between the layers is dominantly odd in momentum and opens a hybridization gap $\propto A$. Here, we have assumed the same effective mass m for electrons and holes, and included only the momentum-independent spin-orbit coupling term Δ_z arising due to bulk inversion asymmetry. We have ignored the asymmetry of the masses and the momentum-dependent spin-orbit coupling terms because they are not essential for understanding the phase diagram of the InAs/GaSb bilayers [11].

The main effect of Coulomb interactions is the binding of the electrons and holes into excitons with the characteristic size d_0 and binding energy E_0 determined by the relation $E_0 = \hbar^2 / (md_0^2) = e^2 / (4\pi\epsilon\epsilon_0 d_0)$ [31]. This leads to an excitonic mean field [11],

$$H_{EC} = \text{Re}[\Delta_1] \tau_y \sigma_y + \text{Re}[\Delta_2] [k_x \tau_x \sigma_z - k_y \tau_y \sigma_0] + \text{Im}[\Delta_1] \tau_x \sigma_y - \text{Im}[\Delta_2] [k_x \tau_y \sigma_z + k_y \tau_x \sigma_0], \quad (2)$$

where Δ_1 and Δ_2 are complex bosonic fields describing s -wave and p -wave excitonic correlations, respectively. For simplicity, we have expanded the fields Δ_1 and Δ_2 only to the lowest order in momentum and neglected the full $|\mathbf{k}|$ dependence, which is present in the numerical solution of the Hartree-Fock equations [11]. It is easy to see by straightforward calculation that the terms on the first line of Eq. (2) obey the TRS $T = i\tau_0 \sigma_y K$ (K is the complex conjugation operator) and the terms in the second line break it. Therefore, the imaginary parts of the fields $\text{Im}[\Delta_1]$, $\text{Im}[\Delta_2] \neq 0$ result in spontaneous TRS breaking.

We can solve the complex bosonic mean fields Δ_1 and Δ_2 by substituting the ansatz Eq. (2) to the Hartree-Fock mean field equations. This way, we arrive at the following mean field equations (see Appendix A for more details):

$$\Delta_1 = \frac{g_s d_0^2}{(2\pi)^2} \int d^2 k [\langle c_{\mathbf{k}\downarrow 2}^\dagger c_{\mathbf{k}\uparrow 1} \rangle - \langle c_{\mathbf{k}\uparrow 2}^\dagger c_{\mathbf{k}\downarrow 1} \rangle] \quad (3)$$

and

$$\Delta_2 = \frac{g_p d_0^4}{(2\pi)^2} \int d^2 k [-\langle c_{\mathbf{k}\uparrow 2}^\dagger c_{\mathbf{k}\uparrow 1} \rangle (k_x - ik_y) + \langle c_{\mathbf{k}\downarrow 2}^\dagger c_{\mathbf{k}\downarrow 1} \rangle (k_x + ik_y)], \quad (4)$$

where g_s (g_p) is the effective interaction strength for s -wave (p -wave) pairing and $c_{1\sigma k}$ ($c_{2\sigma k}$) is the electron annihilation operator with spin σ and momentum k in electron (hole) layer. In our numerical calculations, the integration is performed over the range $|\mathbf{k}| \leq 2.26/d_0$, but the exact values of the integration limits are not important. The effective interaction strengths g_s and g_p can be considered as fitting parameters, whose values should be fixed so one approximately reproduces the results obtained from Hartree-Fock calculations [11].

The values of the model parameters for InAs/GaSb can be estimated by combining theoretical calculations [4,10,11,30] and the experimentally observed energy gaps [7,18]. This way, we arrive at parameter values that are used in our calculations: $E_0/k_B = 200$ K, $d_0 = 10$ nm, $A/(E_0 d_0) = 0.06$, $\Delta_z/E_0 = 0.02$, $g_s/E_0 = 1.0$, and $g_p/E_0 = 0.2$. The band-inversion parameter E_G is a gate-tunable parameter (see Fig. 1), which is varied in our calculations to tune the system from a trivial

insulator to QSH insulator phase. As shown in Fig. 2, our simplified mean field approach, defined by Eqs. (1)–(4), reproduces the results obtained from full Hartree-Fock calculations [11]. For small (large) values of E_G , the system is in a trivial (QSH) insulator phase and, importantly, these two phases are separated from each other by an insulating phase with spontaneously broken TRS, where $\text{Im}[\Delta_1], \text{Im}[\Delta_2] \neq 0$. The bulk gap Δ_{bulk} remains open for all values of E_G because the intermediate TRS broken phase enables the connection of the topologically distinct phases without bulk gap closing. The edge gap Δ_{edge} decreases monotonously when one starts from the trivial phase and tunes the system across the TRS broken phase to the QSH phase, where the gapless edge excitations are protected by the topology. Here, Δ_{bulk} and Δ_{edge} have been computed from the spectra of an infinite system and a wide ribbon with open boundary conditions, respectively. The width of the ribbon $W = 500d_0$ is sufficiently large so the finite size effects are negligible. The formation of the edge gap Δ_{edge} due to the breaking of the TRS occurs in two different ways. The excitonic mean field $\text{Im}[\Delta_1]$ couples the spin-up and spin-down edge modes directly, whereas $\text{Im}[\Delta_2]$ contributes to the gap via a higher order process where it is combined with a spin-orbit coupling term Δ_z and excitonic mean field $\text{Re}[\Delta_1]$.

The appearance of spontaneous TRS breaking can be understood with the help of topological considerations. The topological invariant distinguishing the QSH phase from the trivial insulator can change only if (i) *the bulk energy gap closes* or (ii) *TRS is broken in a regime between the topologically distinct phases*. The case (i) would be the only possibility if the local order were fixed. However, in an interacting system the order parameter corresponds to a minimum of the free energy, and it is energetically favorable to keep the system gapped. Due to this reason, there is a general tendency for the appearance of a TRS broken phase in the transition regime between QSH and trivial insulator phases.

III. LENGTH, TEMPERATURE AND VOLTAGE DEPENDENCE OF THE CONDUCTANCE

The identification of the edge states in InAs/GaSb bilayers was initially problematic due to finite bulk density of states in the minigap [6]. The main breakthrough in eliminating the bulk conduction came from insertion of Si to the interface between the InAs and GaSb layers during the growth process [7]. After achieving a truly insulating bulk this way, Du *et al.* [7] managed to demonstrate in mesoscopic samples wide conductance plateaus quantized to the values expected for nonlocal helical edge transport (variations less than 1%). The accurate conductance quantization was reported for several devices of various lengths and three different geometries in Ref. [7]. Moreover, by imaging the distribution of the current flow inside the sample it has been confirmed that the current flows along the edge in agreement with helical edge conduction [27]. More careful measurements of temperature and voltage dependencies are also consistent with single-mode edge conduction [28]. In a different type of sample, where Si was not inserted and the observed thermal activation gap for the bulk transport is an order of magnitude smaller, multimode edge conduction has been reported by another group [33]. The

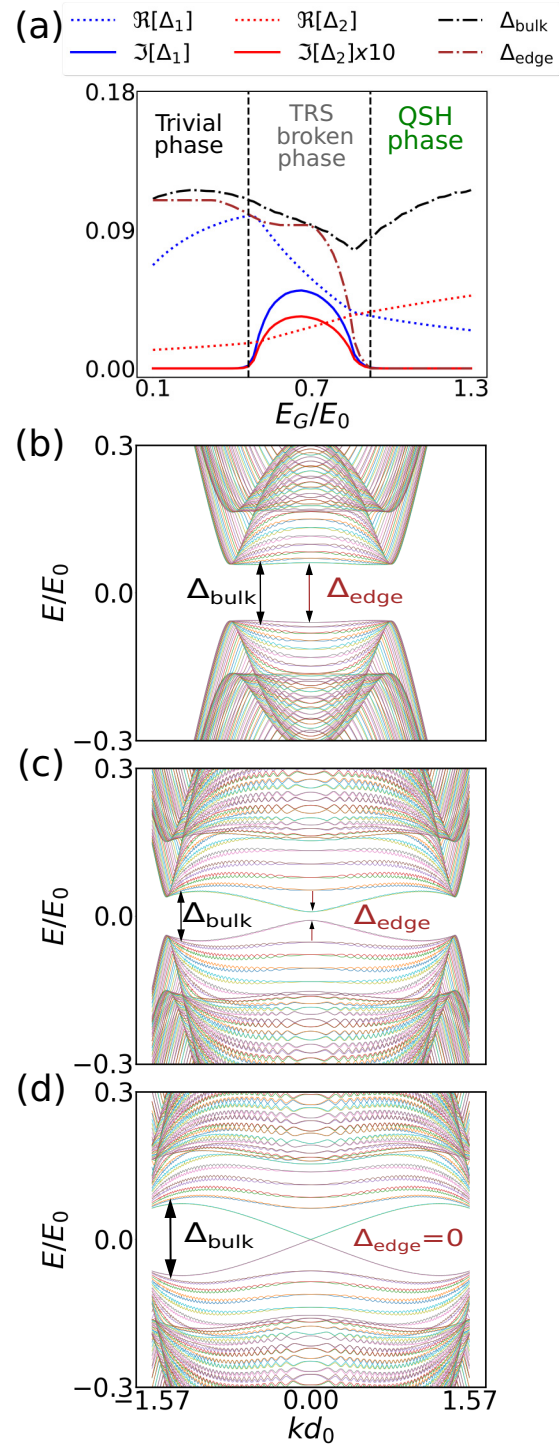


FIG. 2. (a) Phase diagram as a function of E_G . The trivial and QSH phases obey the TRS. In the TRS broken phase, the s - and p -wave excitonic mean fields obey $\text{Im}[\Delta_1], \text{Im}[\Delta_2] \neq 0$. The bulk gap Δ_{bulk} remains open for all values of E_G and the edge gap Δ_{edge} decreases from the bulk gap value to zero, when one tunes E_G across the TRS broken phase toward the QSH phase. The model parameters are described in the text. Energy bands in (b) trivial phase with $E_G = 0.3E_0$, (c) TRS broken phase with $E_G = 0.86E_0$, and (d) QSH phase with $E_G = 1.12E_0$. The eigenenergies are obtained by diagonalizing the tight-binding Hamiltonian which is generated from the continuum Hamiltonian, defined by Eqs. (1)–(4), using the KWANT software package [32].

explanation of the remarkably different transport properties observed in the presence and in absence of Si doping remains an open theoretical problem, but one possible explanation is that there exists additional unprotected edge modes [34] in the absence of Si doping, which are then shifted out of the energy gap in the presence of the Si doping. Because these observations in the two different types of samples are so different that they cannot be explained with the same model Hamiltonian, we concentrate here on the transport experiments in Si-doped samples with a large activation gap [7,28]. We show that these experiments are consistent with the transport properties theoretically obtained in the TRS broken phase.

In long samples, the conductance is not observed to be quantized [7], indicating that backscattering processes occur between the counterpropagating edge channels. It was found that in the limit $eV \gg k_B T$, the resistance is independent on temperature between 20 mK–4.2 K and it increases linearly with the edge length L . These observations are not surprising once the elastic backscattering processes are allowed and large voltage is applied, because under these conditions the inelastic scattering rate is expected to be approximately equal to the elastic one [35] and therefore the localization effects can be neglected and the resistance is expected to be temperature independent. In the QSH phase, the elastic backscattering is forbidden in the presence of TRS due to the topological protection, so these observations are not consistent with the system being in the QSH phase without additional assumptions about the existence of charge puddles that may lead to enhanced backscattering rate [36]. On the other hand, the TRS broken phase supports edge states but the elastic backscattering is now allowed, so the experimental observations are fully consistent with the system being in the TRS broken phase. Thus, the TRS broken phase provides an intrinsic explanation of these experiments, remaining applicable even if we assume that the samples are of high quality so no charge puddles are present in the system.

In short mesoscopic samples with small applied voltage and temperature, the voltage and temperature dependencies of the conductance are more complicated and we need to use a quantum transport approach to describe them. The disorder-averaged differential conductance $G_d = dI/dV$ is obtained from

$$G_d(E_F + eV, T) = \int_{-\infty}^{+\infty} dE \frac{2G_0 \exp[-L/\ell(E)]}{4k_B T \cosh^2 \frac{E-E_F - eV}{2k_B T}}, \quad (5)$$

where $G_0 = e^2/h$, E_F is the Fermi energy, V is voltage, T is temperature of the reservoirs, L is the length of the sample, and $\ell(E)$ is the energy-dependent elastic mean-free path, which for $E \gg \Delta_{\text{edge}}$ is given by [11]

$$\ell(E) = \frac{4a\hbar^2 v^2 E^2}{\xi V_{\text{dis}}^2 \Delta_{\text{edge}}^2}. \quad (6)$$

Here, E is the energy relative to the energy of the crossing of the edge states, v is the edge velocity, V_{dis} is the strength of the disorder potential, ξ is the disorder correlation length, and $a \sim 1$ is a numerical factor. Although the exact expression for $\ell(E)$ is model dependent, it must always satisfy $\ell(E) \rightarrow \infty$ for $E \gg \Delta_{\text{edge}}$, so $G_d \approx 2G_0$ for $k_B T \gg \Delta_{\text{edge}}$. Therefore,

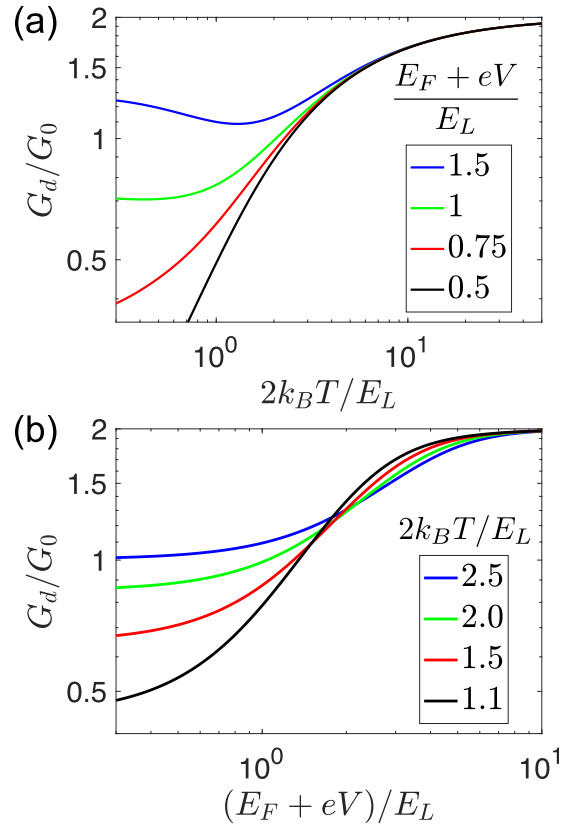


FIG. 3. (a) Differential conductance G_d as a function of T for $(E_F + eV)/E_L = 1.5, 1, 0.75, 0.5$. (b) G_d as a function of V for $2k_B T/E_L = 2.5, 2, 1.5, 1.1$.

there exists robust asymptotic limits

$$G_d \approx \begin{cases} 2G_0[1 - L/\ell(E_F + eV)], & k_B T \ll E_F + eV, \\ 2G_0, & k_B T \gg \Delta_{\text{edge}}, \end{cases} \quad (7)$$

which guarantee that G_d undergoes a crossover from non-quantized value to the quantized value $G_d = 2G_0$, both with increasing temperature and voltage.

To study the full temperature dependence, we introduce an energy scale E_L , which is defined in such a way that

$$\ell(E_L) \equiv L, \text{ i.e. } E_L = \sqrt{\frac{L\xi V_{\text{dis}}^2 \Delta_{\text{edge}}^2}{4a\hbar^2 v^2}}. \quad (8)$$

The differential conductance G_d , which depends on two parameters $(E_F + eV)/E_L$ and $2k_B T/E_L$, is shown in Fig. 3. In this analysis, we have neglected the effects of electron-electron interactions beyond the mean-field theory and the energy and temperature dependence of the excitonic mean fields. Nevertheless, our results for the G_d crossovers from a nonquantized to the quantized value $G_d = 2G_0$ with increasing voltage and temperature are in reasonable agreement with the experimental observations [28]. We consider the observations of these crossovers as very strong evidence of single-mode edge transport.

In the experiment [28], the temperature dependence of the conductance

$$G(E_F, V, T) = \frac{1}{V} \int_0^V dV G_d(E_F + eV, T) \quad (9)$$

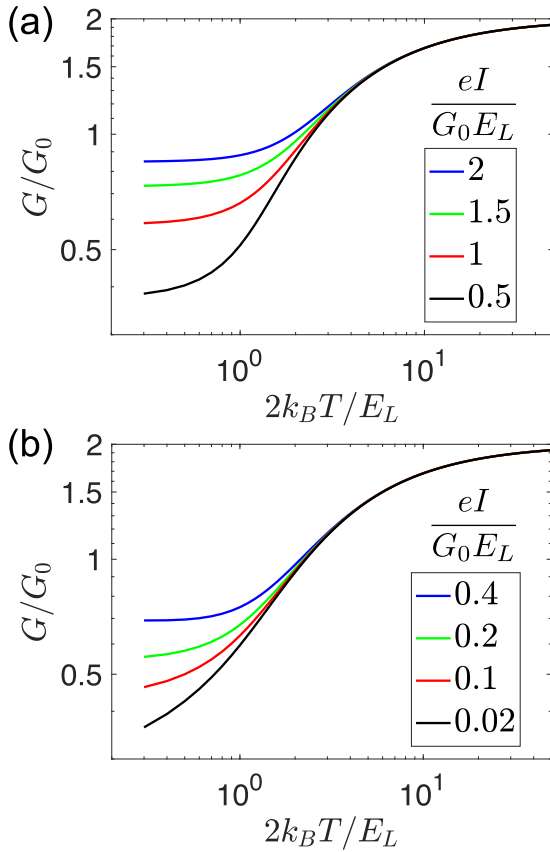


FIG. 4. (a) Conductance G as a function of T for $E_F = 0$ and $eI/(G_0 E_L) = 2, 1.5, 1, 0.5$. (b) Same for $E_F/E_L = 0.7$ and $eI/(G_0 E_L) = 0.4, 0.2, 0.1, 0.02$.

was reported also in a current I biased situation. The theoretical predictions for this situation, obtained using Eqs. (5), (6), (9), and $I = GV$, are shown in Fig. 4. In this case, the shapes of the curves in the crossover regime depend on the Fermi energy E_F and they resemble the experimental observations [28] more in the case of reasonably large values of E_F . In a more detailed microscopic description, the crossing of the edge states may be buried within the bulk bands [37,38] so reasonably large E_F compared the energy of the crossing could naturally be realized in the experiments.

The qualitative features observed in the transport experiments discussed above have been previously explained using various different mechanisms. The advantage of our approach is that a single mechanism provides a unified and comprehensive explanation for all these observations and this mechanism is also consistent with the other evidence of excitonic phenomenology in InAs/GaSb quantum wells [18–22]. We point out that the experimentally observed crossovers as a function of voltage and current already show clear saturation toward the quantized value [28], but the observation of an equally clear signature as a function of temperature may require optimization of the sample size because the saturation should occur at sufficiently low temperature so thermally activated bulk transport does not contribute significantly to the conductance. The quantitative comparison to the experiments goes beyond the scope of this paper because, in the crossover regime, the conductance depends on the Luttinger parameter

describing the interactions at the edge and the temperature and energy dependencies of the excitonic mean fields. We expect that once these effects are taken into account, our theory provides a reasonably good quantitative description of all the transport regimes as a function of temperature, voltage, current, and sample size.

IV. DECOUPLING OF BULK AND EDGE TRANSPORT IN CORBINO GEOMETRY

We have shown that the transport experiments performed so far with InAs/GaSb devices are consistent with the system being in the TRS broken phase. However, it is difficult to rule out other theoretical explanations [36,39–43] based on these experimental observations. In this section, we propose a transport experiment, which could be used to prove the existence of the exotic TRS broken phase based on robust topological arguments. This kind of experiment would also directly probe the main difference between the transport theories because our theory is so far the only proposal where the backscattering originates from the spontaneous TRS breaking in the bulk.

For this purpose, we consider a Corbino device where the differential conductances corresponding to the bulk G_{bulk} and edge G_{edge} transport can be decoupled as illustrated in Fig. 5. The dimensions of the Corbino disk $R_{\text{in}} \approx 1 \mu\text{m}$ and $R_{\text{out}} = 2 \mu\text{m}$ are chosen so the transport is (approximately) ballistic and the decay lengths of the evanescent bulk modes in the middle of the bulk gap are much shorter than the transport paths. This guarantees that $G_{\text{bulk}} \approx 0$ for the applied voltage satisfying $|eV_{dc}| < \Delta_{\text{bulk}}/2$. Importantly, this allows us to demonstrate that the transport gap does not close when the system is tuned from trivial to the QSH insulator phase by varying E_G [see Fig. 5(b)]. On the other hand, the edge conductance changes smoothly from $G_{\text{edge}} = 0$ (trivial phase) to $G_{\text{edge}} = 2G_0$ (QSH phase) upon increasing E_G , demonstrating the closing of the edge gap Δ_{edge} at the transition to the QSH insulator phase [see Fig. 5(c)]. Importantly, the bulk and edge conductances can be elegantly measured in the same device when the system is tuned *in situ* from the trivial to the QSH insulator phase using the gate voltages. Such kind of experimental demonstration of a topological transition without a bulk transport gap closing would constitute proof of the existence of TRS broken insulating phase.

In Appendices B and C, we consider the effects of mass asymmetry and disorder on the bulk and edge conductances in the Corbino device. We find that although the high-energy bulk transport is significantly affected by these effects, all the important qualitative features in the low-energy transport are robust also in the presence of large mass asymmetry and strong disorder.

V. CONCLUSIONS AND DISCUSSION

We have discussed the possibility of unconventional topological phase transition between trivial and QSH insulator phases in band-inverted electron-hole bilayers. The hallmark of this transition is the existence of an intermediate insulating phase with spontaneously broken TRS. We have demonstrated that the transport properties of the system in the TRS broken phase are consistent with the observed transport

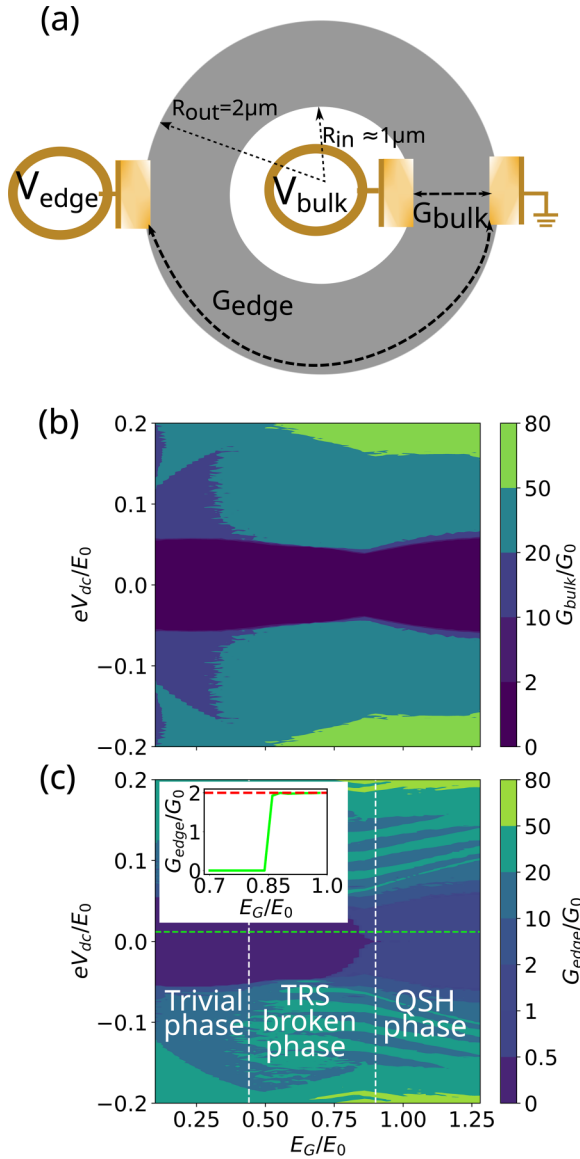


FIG. 5. (a) Schematic illustration of a Corbino device and the transport paths corresponding to the bulk and edge differential conductances G_{bulk} and G_{edge} . The dimensions of the Corbino disk $R_{\text{in}} \approx 1 \mu\text{m}$ and $R_{\text{out}} = 2 \mu\text{m}$ are chosen so the transport is (approximately) ballistic and the decay lengths of the evanescent bulk modes in the middle of the bulk gap are much shorter than the transport paths. (b), (c) G_{bulk} and G_{edge} as a function of E_G and applied voltage V_{dc} . The inset in (c) shows G_{edge} as a function of E_G (green line) for $eV_{\text{dc}} = 0.012E_0$. The red dashed line is a guide to the eye. The conductances have been calculated with the help of the tight-binding Hamiltonian which is generated from the continuum Hamiltonian, defined by Eqs. (1)–(4), using the KWANT software package [32].

characteristics of InAs/GaSb devices, and we have shown that the measurement of the bulk and edge conductances in a Corbino device can provide unambiguous transport signatures of a topological transition without a bulk transport gap closing, proving the existence of the TRS broken phase. In this paper, we have demonstrated that because of the TRS broken phase the edge becomes smoothly conducting when one tunes the system from the trivial to the QSH insulator phase, and

we expect similar smooth transitions also in other observables related to the topological invariant. For example, the spin Hall conductivity is expected to change smoothly in the case of unconventional transition via the TRS broken phase although it changes abruptly in the case of a conventional transition with a bulk gap closing. We expect that the spontaneous TRS breaking would also show up in the spectrum of the collective modes. In this work we have assumed that the disorder is not so strong that it would influence the excitonic mean fields, but we think that the investigation of the effect of strong disorder on the appearance of the spontaneous TRS breaking would be an important direction for future research.

Although we have focused on InAs/GaSb bilayers, we point out that band-inverted electron-hole systems can be realized in many semiconducting bilayers by creating a strong electric field at the barrier between the layers [44–48]. In principle, all these systems are potential candidates for supporting the interplay of excitonic correlations and the QSH effect, but for most of the semiconductors the barrier thickness may have to be so large that the hybridization gap between the electron and hole bands becomes too small to realize a sufficiently large topological gap in the QSH insulator phase. Our theory may also be applicable to HgTe bilayers [12].

Finally, we point out that if an insulating barrier is inserted between the electron and hole layers to suppress the tunneling between the layers, the excitonic correlations can be probed also with the help of a Josephson-like tunneling anomaly and counterflow supercurrents as demonstrated in quantum Hall exciton condensates [49–54] and more recently in double bilayer graphene systems where the exciton condensate is realized in the absence of magnetic field [55–57]. The tunneling barrier also allows us to study the physics discussed in this paper in more detail because it affects the competition between the s -wave and p -wave excitonic mean fields and the appearance of the TRS broken phase [11].

In a separate work [58], we show that in the presence of induced superconductivity the spontaneous TRS breaking allows us to realize Majorana zero modes in the absence of magnetic field.

ACKNOWLEDGMENTS

We thank D. I. Pikulin for useful discussions and comments. The paper is supported by the Foundation for Polish Science through the IRA Programme cofinanced by EU within SG OP and the Academy of Finland Project No. 331094. We acknowledge the computational resources provided by the Aalto Science-IT project and the access to the computing facilities of the Interdisciplinary Center of Modeling at the University of Warsaw, Grants No. GB82-13, No. G78-13, and No. G75-10.

APPENDIX A: MINIMAL MODEL AND MEAN-FIELD EQUATIONS FOR EXCITONIC CORRELATIONS

Based on the numerical solution of the Hartree-Fock mean field theory [11], we know that the main effect of intraband interactions (in the relevant part of the parameter space) is to renormalize the band structure. Therefore, we consider only

the interband interactions

$$\hat{H}_I = - \sum_{s,s'} \sum_{\mathbf{k},\mathbf{k}'} V_{\mathbf{k},\mathbf{k}'} c_{\mathbf{k}s1}^\dagger c_{\mathbf{k}s'2} c_{\mathbf{k}'s'2}^\dagger c_{\mathbf{k}'s1}, \quad (\text{A1})$$

where $V_{\mathbf{k},\mathbf{k}'}$ describes the Coulomb interactions between the layers. On a mean-field level, the Hamiltonian is

$$\hat{H}_{\text{mf}} = \hat{H}_0 - \sum_{\mathbf{k},s,s'} [\Delta_{s,s'}(\mathbf{k}) c_{\mathbf{k}s1}^\dagger c_{\mathbf{k}s'2} + \text{H.c.}], \quad (\text{A2})$$

where

$$\Delta_{s,s'}(\mathbf{k}) = \sum_{\mathbf{k}'} V_{\mathbf{k},\mathbf{k}'} f_{s,s'}(\mathbf{k}'), \quad (\text{A3})$$

$$f_{s,s'}(\mathbf{k}) \equiv \langle c_{\mathbf{k}s'2}^\dagger c_{\mathbf{k}s1} \rangle = \sum_m n_F(E_{m\mathbf{k}}) [U_{\mathbf{k}} Q_{ss'} U_{\mathbf{k}}^\dagger]_{mm}, \quad (\text{A4})$$

$$Q_{\uparrow\uparrow} = \begin{pmatrix} 0 & 0 & 0 & 0 \\ 0 & 0 & 0 & 0 \\ 1 & 0 & 0 & 0 \\ 0 & 0 & 0 & 0 \end{pmatrix}, \quad Q_{\downarrow\downarrow} = \begin{pmatrix} 0 & 0 & 0 & 0 \\ 0 & 0 & 0 & 0 \\ 0 & 0 & 0 & 0 \\ 1 & 0 & 0 & 0 \end{pmatrix},$$

$$Q_{\downarrow\uparrow} = \begin{pmatrix} 0 & 0 & 0 & 0 \\ 0 & 0 & 0 & 0 \\ 0 & 1 & 0 & 0 \\ 0 & 0 & 0 & 0 \end{pmatrix}, \quad Q_{\uparrow\downarrow} = \begin{pmatrix} 0 & 0 & 0 & 0 \\ 0 & 0 & 0 & 0 \\ 0 & 0 & 0 & 0 \\ 0 & 1 & 0 & 0 \end{pmatrix}, \quad (\text{A5})$$

$n_F(E) = (e^{E/(k_B T)} + 1)^{-1}$ is the Fermi function, T is the temperature, and the transformation $U_{\mathbf{k}}$ diagonalizes

$$\text{diag}(E_{1\mathbf{k}}, E_{2\mathbf{k}}, E_{3\mathbf{k}}, E_{4\mathbf{k}}) = U_{\mathbf{k}} H_{\text{mf}}(\mathbf{k}) U_{\mathbf{k}}^\dagger, \quad (\text{A6})$$

the mean-field Hamiltonian:

$$H_{\text{mf}}(\mathbf{k}) = \begin{pmatrix} \frac{\hbar^2 k^2}{2m} - E_G & 0 & (A + \Delta_2)(k_x + ik_y) & -(\Delta_1 + \Delta_2) \\ 0 & \frac{\hbar^2 k^2}{2m} - E_G & (\Delta_1 + \Delta_2) & -(A + \Delta_2)(k_x - ik_y) \\ (A + \Delta_2)^*(k_x - ik_y) & (\Delta_1 + \Delta_2)^* & E_G - \frac{\hbar^2 k^2}{2m} & 0 \\ -(\Delta_1 + \Delta_2)^* & -(A + \Delta_2)^*(k_x + ik_y) & 0 & E_G - \frac{\hbar^2 k^2}{2m} \end{pmatrix}. \quad (\text{A7})$$

Here we have utilized the fact that the excitonic mean field can be approximated as

$$\Delta^{\text{mf}} = i\Delta_1\sigma_2 - \Delta_2(k_x\sigma_3 + ik_y\sigma_0), \quad (\text{A8})$$

where Δ_1 and Δ_2 are complex bosonic fields describing s -wave and p -wave excitonic correlations, respectively.

By inverting the interaction matrix and substituting the ansatz Eq. (A8) to the mean-field equation, we obtain

$$\frac{d_0^2}{L^2} \sum_{\mathbf{k}} [f_{\uparrow,\downarrow}(\mathbf{k}) - f_{\downarrow,\uparrow}(\mathbf{k})] = 2 \frac{d_0^2}{L^2} \sum_{\mathbf{k},\mathbf{k}'} V_{\mathbf{k}\mathbf{k}'}^{-1} \Delta_1 = \frac{1}{g_s} \Delta_1 \quad (\text{A9})$$

and

$$\frac{d_0^2}{L^2} \sum_{\mathbf{k}} [-f_{\uparrow,\uparrow}(\mathbf{k})(k_x - ik_y) + f_{\downarrow,\downarrow}(\mathbf{k})(k_x + ik_y)] = 2 \frac{d_0^2}{L^2} \sum_{\mathbf{k},\mathbf{k}'} V_{\mathbf{k},\mathbf{k}'}^{-1} \Delta_2 (k_x k'_x + k_y k'_y) = \frac{1}{g_p d_0^2} \Delta_2, \quad (\text{A10})$$

where we have defined effective interaction strengths g_s and g_p for the s -wave and p -wave excitonic correlations as

$$g_s^{-1} = 2 \frac{d_0^2}{L^2} \sum_{\mathbf{k},\mathbf{k}'} V_{\mathbf{k},\mathbf{k}'}^{-1}, \quad g_p^{-1} = 2 \frac{d_0^4}{L^2} \sum_{\mathbf{k},\mathbf{k}'} V_{\mathbf{k},\mathbf{k}'}^{-1} (k_x k'_x + k_y k'_y). \quad (\text{A11})$$

The length scale d_0 is introduced to guarantee that the interaction strengths have a unit of energy, and it can in principle be chosen arbitrarily. However, we know that in the case of Coulomb interaction the natural length d_0 and energy E_0 scales are determined so the kinetic and interaction energies are equal:

$$E_0 = \frac{\hbar^2}{d_0^2} \frac{1}{m} = \frac{1}{4\pi\epsilon\epsilon_0} \frac{e^2}{d_0}. \quad (\text{A12})$$

This way, we obtain the mean field Eqs. (3) and (4) given in the main text.

APPENDIX B: EFFECTS OF EFFECTIVE MASS ASYMMETRY ON THE TRANSPORT CHARACTERISTICS IN THE CORBINO DEVICES

In typical semiconductors, the effective masses of the electrons m_e and holes m_h are different. It was shown in Ref. [11] that this does not influence the phase diagram of InAs/GaSb

bilayer qualitatively if one uses the first-principle estimate for the effective mass asymmetry $m_e/m_h = 0.84$ [30]. Here, we study the effects of the effective mass asymmetry on the results reported in the main text of this paper.

In the presence of the effective mass asymmetry, the exciton binding energy and radius are determined from the equation

$$E_0 = \frac{\hbar^2}{2m_{\text{eff}} d_0^2} = \frac{1}{4\pi\epsilon\epsilon_0} \frac{e^2}{d_0}, \quad (\text{B1})$$

where the reduced mass m_{eff} satisfies equation $m_{\text{eff}}^{-1} = m_e^{-1} + m_h^{-1}$. Moreover, the mean-field Hamiltonian can be written as

$$H_{\text{mf}}(\mathbf{k}) = \begin{pmatrix} \frac{\hbar^2 k^2}{2m_e} - \frac{2m_{\text{eff}}}{m_e} E_G & 0 & (A + \Delta_2)(k_x + ik_y) & -(\Delta_1 + \Delta_z) \\ 0 & \frac{\hbar^2 k^2}{2m_e} - \frac{2m_{\text{eff}}}{m_e} E_G & (\Delta_1 + \Delta_z) & -(A + \Delta_2)(k_x - ik_y) \\ (A + \Delta_2)^*(k_x - ik_y) & (\Delta_1 + \Delta_z)^* & \frac{2m_{\text{eff}}}{m_h} E_G - \frac{\hbar^2 k^2}{2m_h} & 0 \\ -(\Delta_1 + \Delta_z)^* & -(A + \Delta_2)^*(k_x + ik_y) & 0 & \frac{2m_{\text{eff}}}{m_h} E_G - \frac{\hbar^2 k^2}{2m_h} \end{pmatrix}. \quad (\text{B2})$$

Notice that if $m_e = m_h = m$, we obtain $m_{\text{eff}} = m/2$, and therefore these equations reduce back to the equations considered in the main text. Moreover, we have defined E_G analogously with the earlier analysis: tuning E_G allows us to vary the electron and hole densities so they remain equal to each other.

The transport characteristics in the Corbino geometry for $m_e/m_h = 0.84, 0.3$ are shown in Fig. 6. By comparing Fig. 6 to Fig. 5, we conclude that the low-energy transport characteristics are unaffected by the effective mass asymmetry, but the asymmetry leads to visible changes in the bulk conductance at high energies.

APPENDIX C: EFFECTS OF DISORDER ON THE TRANSPORT CHARACTERISTICS IN THE CORBINO DEVICES

In Ref. [11], it was shown that in the presence of spontaneous TRS breaking the nonmagnetic disorder can cause backscattering. The more detailed length, temperature, and voltage dependence of the conductance in the presence of the disorder was discussed in Sec. III. In Sec. IV, we concentrated on the transport characteristics in mesoscopic Corbino devices where the mean-free path of the edge modes is longer than the distance between the contacts but the decay length of

the evanescent bulk modes in the middle of the gap is much shorter than the width of the Corbino ring. In such kind of situation, we expect that the disorder is unimportant for the low-energy transport characteristics but it can influence the conductance at energies above the bulk gap. In this Appendix, we explicitly calculate the effects of a disorder potential on the conductances in this geometry by modeling the disorder as uncorrelated uniformly distributed on-site energies between $[-V_{\text{dis}}, V_{\text{dis}}]$. We assume that the disorder is not so strong that it would influence the excitonic mean fields. In particular, this assumption is justified in the range of the disorder strengths where the effects of the disorder can be treated using the self-consistent Born approximation [59,60], because in this case the disorder just renormalizes the band structure parameters so the phase diagram remains qualitatively the same.

In Fig. 7, we show the edge and bulk conductance as a function of E_G and eV_{dc} in the case of moderate $V_{\text{dis}} = 0.1E_0$ and strong $V_{\text{dis}} = 0.5E_0$ disorder strengths. The results show that the main qualitative transport features, i.e., the bulk gap remains open while the edge gap smoothly decreases to zero in the TRS-broken phase, can be observed also in the presence of strong disorder. The bulk conductance is

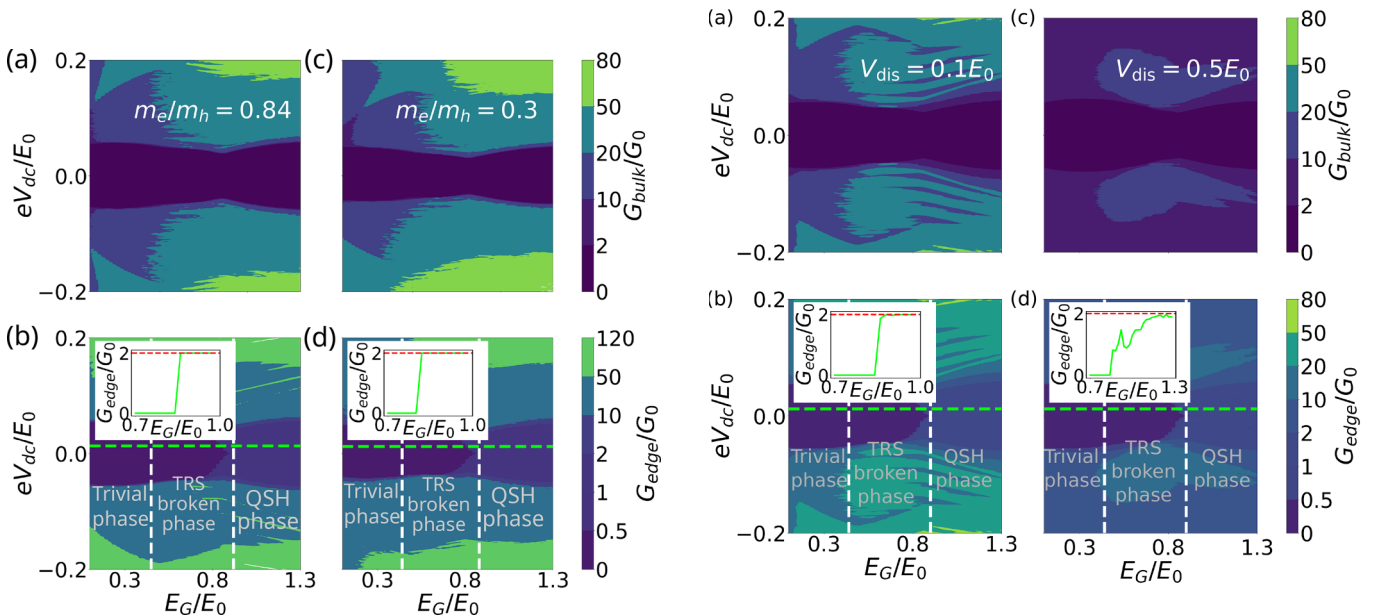


FIG. 6. G_{bulk} and G_{edge} for the Corbino geometry shown in Fig. 5 as a function of E_G and V_{dc} calculated for different values of mass asymmetry: (a), (b) $m_e/m_h = 0.84$ and (c), (d) $m_e/m_h = 0.30$. The insets show G_{edge} as a function of E_G for small eV_{dc} (green line). We have used $eV_{\text{dc}} = 0.013E_0$ in (b) and $eV_{\text{dc}} = 0.012E_0$ in (d).

FIG. 7. G_{bulk} and G_{edge} for the Corbino geometry shown in Fig. 5 as a function of E_G and V_{dc} calculated for different values of the disorder strength: (a), (b) $V_{\text{dis}} = 0.1E_0$ and (c), (d) $V_{\text{dis}} = 0.5E_0$. The insets show G_{edge} as a function of E_G for $eV_{\text{dc}} = 0.012E_0$ (green lines). The conductances have been calculated by taking the average over 20 disorder realizations.

significantly affected by the disorder in both cases. On the other hand, in the case of moderate disorder strength the edge conductance remains practically identical to the clean case,

whereas in the case of strong disorder the interval of E_G where the conductance increases from 0 to the quantized value is extended.

-
- [1] M. Z. Hasan and C. L. Kane, Colloquium: Topological insulators, *Rev. Mod. Phys.* **82**, 3045 (2010).
- [2] X.-L. Qi and S.-C. Zhang, Topological insulators and superconductors, *Rev. Mod. Phys.* **83**, 1057 (2011).
- [3] B. A. Bernevig, T. L. Hughes, and S.-C. Zhang, Quantum spin Hall effect and topological phase transition in HgTe quantum wells, *Science* **314**, 1757 (2006).
- [4] C. Liu, T. L. Hughes, X.-L. Qi, K. Wang, and S.-C. Zhang, Quantum Spin Hall Effect in Inverted Type-II Semiconductors, *Phys. Rev. Lett.* **100**, 236601 (2008).
- [5] M. König, S. Wiedmann, C. Brüne, A. Roth, H. Buhmann, L. W. Molenkamp, X.-L. Qi, and S.-C. Zhang, Quantum spin Hall insulator state in HgTe quantum wells, *Science* **318**, 766 (2007).
- [6] I. Knez, R.-R. Du, and G. Sullivan, Evidence for Helical Edge Modes in Inverted InAs/GaSb Quantum Wells, *Phys. Rev. Lett.* **107**, 136603 (2011).
- [7] L. Du, I. Knez, G. Sullivan, and R.-R. Du, Robust Helical Edge Transport in Gated InAs/GaSb Bilayers, *Phys. Rev. Lett.* **114**, 096802 (2015).
- [8] S. Wu, V. Fatemi, Q. D. Gibson, K. Watanabe, T. Taniguchi, R. J. Cava, and P. Jarillo-Herrero, Observation of the quantum spin Hall effect up to 100 kelvin in a monolayer crystal, *Science* **359**, 76 (2018).
- [9] Y. Lozovik and V. Yudson, New mechanism for superconductivity: Pairing between spatially separated electrons and holes, *Sov. Phys. JETP* **44**, 389 (1976).
- [10] Y. Naveh and B. Laikhtman, Excitonic Instability and Electric-Field-Induced Phase Transition Towards a Two-Dimensional Exciton Condensate, *Phys. Rev. Lett.* **77**, 900 (1996).
- [11] D. I. Pikulin and T. Hyart, Interplay of Exciton Condensation and the Quantum Spin Hall Effect in InAs/GaSb Bilayers, *Phys. Rev. Lett.* **112**, 176403 (2014).
- [12] J. C. Budich, B. Trauzettel, and P. Michetti, Time Reversal Symmetric Topological Exciton Condensate in Bilayer HgTe Quantum Wells, *Phys. Rev. Lett.* **112**, 146405 (2014).
- [13] L.-H. Hu, C.-C. Chen, C.-X. Liu, F.-C. Zhang, and Y. Zhou, Topological charge-density and spin-density waves in InAs/GaSb quantum wells under an in-plane magnetic field, *Phys. Rev. B* **96**, 075130 (2017).
- [14] F. Xue and A. H. MacDonald, Time-Reversal Symmetry-Breaking Nematic Insulators Near Quantum Spin Hall Phase Transitions, *Phys. Rev. Lett.* **120**, 186802 (2018).
- [15] Q. Zhu, M. W.-Y. Tu, Q. Tong, and W. Yao, Gate tuning from exciton superfluid to quantum anomalous Hall in van der Waals heterobilayer, *Sci. Adv.* **5**, eaau6120 (2019).
- [16] D. Varsano, M. Palummo, E. Molinari, and M. Rontani, A monolayer transition-metal dichalcogenide as a topological excitonic insulator, *Nat. Nanotechnol.* **15**, 367 (2020).
- [17] Y. Zeng, F. Xue, and A. H. MacDonald, In-plane magnetic field induced density wave states near quantum spin Hall phase transitions, *Phys. Rev. B* **105**, 125102 (2022).
- [18] L. Du, X. Li, W. Lou, G. Sullivan, K. Chang, J. Kono, and R.-R. Du, Evidence for a topological excitonic insulator in InAs/GaSb bilayers, *Nat. Commun.* **8**, 1971 (2017).
- [19] X. Wu, W. Lou, K. Chang, G. Sullivan, and R.-R. Du, Resistive signature of excitonic coupling in an electron-hole double layer with a middle barrier, *Phys. Rev. B* **99**, 085307 (2019).
- [20] X.-J. Wu, W. Lou, K. Chang, G. Sullivan, A. Ikhlassi, and R.-R. Du, Electrically tuning many-body states in a Coulomb-coupled InAs/InGaSb double layer, *Phys. Rev. B* **100**, 165309 (2019).
- [21] D. Xiao, C.-X. Liu, N. Samarth, and L.-H. Hu, Anomalous Quantum Oscillations of Interacting Electron-Hole Gases in Inverted Type-II InAs/GaSb Quantum Wells, *Phys. Rev. Lett.* **122**, 186802 (2019).
- [22] H. Irie, T. Akiho, F. Couëdo, K. Suzuki, K. Onomitsu, and K. Muraki, Energy gap tuning and gate-controlled topological phase transition in InAs/In_xGa_{1-x}Sb composite quantum wells, *Phys. Rev. Mater.* **4**, 104201 (2020).
- [23] Y. Jia, P. Wang, C.-L. Chiu, Z. Song, G. Yu, B. Jäck, S. Lei, S. Klemenž, F. A. Cevallos, M. Onyszczyk, N. Fishchenko, X. Liu, G. Farahi, F. Xie, Y. Xu, K. Watanabe, T. Taniguchi, B. A. Bernevig, R. J. Cava, L. M. Schoop *et al.*, Evidence for a monolayer excitonic insulator, *Nat. Phys.* **18**, 87 (2022).
- [24] B. Sun, W. Zhao, T. Palomaki, Z. Fei, E. Runburg, P. Malinowski, X. Huang, J. Cenker, Y.-T. Cui, J.-H. Chu, X. Xu, S. S. Ataei, D. Varsano, M. Palummo, E. Molinari, M. Rontani, and D. H. Cobden, Evidence for equilibrium exciton condensation in monolayer WTe₂, *Nat. Phys.* **18**, 94 (2022).
- [25] F. Qu, A. J. A. Beukman, S. Nadj-Perge, M. Wimmer, B.-M. Nguyen, W. Yi, J. Thorp, M. Sokolich, A. A. Kiselev, M. J. Manfra, C. M. Marcus, and L. P. Kouwenhoven, Electric and Magnetic Tuning Between the Trivial and Topological Phases in InAs/GaSb Double Quantum Wells, *Phys. Rev. Lett.* **115**, 036803 (2015).
- [26] I. Knez, C. T. Rettner, S.-H. Yang, S. S. P. Parkin, L. Du, R.-R. Du, and G. Sullivan, Observation of Edge Transport in the Disordered Regime of Topologically Insulating InAs/GaSb Quantum Wells, *Phys. Rev. Lett.* **112**, 026602 (2014).
- [27] E. M. Spanton, K. C. Nowack, L. Du, G. Sullivan, R.-R. Du, and K. A. Moler, Images of Edge Current in InAs/GaSb Quantum Wells, *Phys. Rev. Lett.* **113**, 026804 (2014).
- [28] T. Li, P. Wang, H. Fu, L. Du, K. A. Schreiber, X. Mu, X. Liu, G. Sullivan, G. A. Csáthy, X. Lin, and R.-R. Du, Observation of a Helical Luttinger Liquid in InAs/GaSb Quantum Spin Hall Edges, *Phys. Rev. Lett.* **115**, 136804 (2015).
- [29] B.-M. Nguyen, A. A. Kiselev, R. Noah, W. Yi, F. Qu, A. J. A. Beukman, F. K. de Vries, J. van Veen, S. Nadj-Perge, L. P. Kouwenhoven, M. Kjaergaard, H. J. Suominen, F. Nichele, C. M. Marcus, M. J. Manfra, and M. Sokolich, Decoupling Edge Versus Bulk Conductance in the Trivial Regime of an InAs/GaSb Double Quantum Well using Corbino Ring Geometry, *Phys. Rev. Lett.* **117**, 077701 (2016).
- [30] C. Liu and S. Zhang, Models and materials for topological insulators, in *Topological Insulators*, edited by M. Franz and L. Molenkamp, Contemporary Concepts of Condensed Matter Science, Vol. 6 (Elsevier, 2013), Chap. 3, pp. 59–89.

- [31] X. Zhu, P. B. Littlewood, M. S. Hybertsen, and T. M. Rice, Exciton Condensate in Semiconductor Quantum Well Structures, *Phys. Rev. Lett.* **74**, 1633 (1995).
- [32] C. W. Groth, M. Wimmer, A. R. Akhmerov, and X. Waintal, Kwant: A software package for quantum transport, *New J. Phys.* **16**, 063065 (2014).
- [33] F. Nichele, H. J. Suominen, M. Kjaergaard, C. M. Marcus, E. Sajadi, J. A. Folk, F. Qu, A. J. A. Beukman, F. K. de Vries, J. van Veen, S. Nadj-Perge, L. P. Kouwenhoven, B.-M. Nguyen, A. A. Kiselev, W. Yi, M. Sokolich, M. J. Manfra, E. M. Spanton, and K. A. Moler, Edge transport in the trivial phase of InAs/GaSb, *New J. Phys.* **18**, 083005 (2016).
- [34] N. M. Nguyen, G. Cuono, R. Islam, C. Autieri, T. Hyart, and W. Brzezicki, Unprotected edge modes in quantum spin Hall insulator candidate materials, [arXiv:2209.06912](https://arxiv.org/abs/2209.06912).
- [35] D. A. Bagrets, I. V. Gornyi, and D. G. Polyakov, Nonequilibrium kinetics of a disordered Luttinger liquid, *Phys. Rev. B* **80**, 113403 (2009).
- [36] J. I. Väyrynen, M. Goldstein, Y. Gefen, and L. I. Glazman, Resistance of helical edges formed in a semiconductor heterostructure, *Phys. Rev. B* **90**, 115309 (2014).
- [37] R. Skolasinski, D. I. Pikulin, J. Alicea, and M. Wimmer, Robust helical edge transport in quantum spin Hall quantum wells, *Phys. Rev. B* **98**, 201404(R) (2018).
- [38] C.-A. Li, S.-B. Zhang, and S.-Q. Shen, Hidden edge Dirac point and robust quantum edge transport in InAs/GaSb quantum wells, *Phys. Rev. B* **97**, 045420 (2018).
- [39] Y. Tanaka, A. Furusaki, and K. A. Matveev, Conductance of a Helical Edge Liquid Coupled to a Magnetic Impurity, *Phys. Rev. Lett.* **106**, 236402 (2011).
- [40] J. C. Budich, F. Dolcini, P. Recher, and B. Trauzettel, Phonon-Induced Backscattering in Helical Edge States, *Phys. Rev. Lett.* **108**, 086602 (2012).
- [41] A. M. Lunde and G. Platero, Helical edge states coupled to a spin bath: Current-induced magnetization, *Phys. Rev. B* **86**, 035112 (2012).
- [42] A. Del Maestro, T. Hyart, and B. Rosenow, Backscattering between helical edge states via dynamic nuclear polarization, *Phys. Rev. B* **87**, 165440 (2013).
- [43] G. Dolcetto, M. Sassetti, and T. L. Schmidt, Edge physics in two-dimensional topological insulators, *Riv. Nuovo Cimento* **39**, 113 (2016).
- [44] U. Sivan, P. M. Solomon, and H. Shtrikman, Coupled Electron-Hole Transport, *Phys. Rev. Lett.* **68**, 1196 (1992).
- [45] B. E. Kane, J. P. Eisenstein, W. Wegscheider, L. N. Pfeiffer, and K. W. West, Separately contacted electron-hole double layer in a GaAs/Al_xGa_{1-x}As heterostructure, *Appl. Phys. Lett.* **65**, 3266 (1994).
- [46] S. Shapira, E. H. Linfield, and M. Pepper, A simple lateral transport device of strongly interacting electron and hole layers, *Appl. Phys. Lett.* **74**, 1603 (1999).
- [47] M. Pohl, M. Lynass, J. G. S. Lok, W. Dietsche, K. v. Klitzing, K. Eberl, and R. Mühle, Closely spaced and separately contacted two-dimensional electron and hole gases by in situ focused-ion implantation, *Appl. Phys. Lett.* **80**, 2105 (2002).
- [48] J. A. Seamons, D. R. Tibbetts, J. L. Reno, and M. P. Lilly, Undoped electron-hole bilayers in a GaAs/AlGaAs double quantum well, *Appl. Phys. Lett.* **90**, 052103 (2007).
- [49] I. B. Spielman, J. P. Eisenstein, L. N. Pfeiffer, and K. W. West, Resonantly Enhanced Tunneling in a Double Layer Quantum Hall Ferromagnet, *Phys. Rev. Lett.* **84**, 5808 (2000).
- [50] I. B. Spielman, J. P. Eisenstein, L. N. Pfeiffer, and K. W. West, Observation of a Linearly Dispersing Collective Mode in a Quantum Hall Ferromagnet, *Phys. Rev. Lett.* **87**, 036803 (2001).
- [51] Y. Yoon, L. Tiemann, S. Schmult, W. Dietsche, K. von Klitzing, and W. Wegscheider, Interlayer Tunneling in Counterflow Experiments on the Excitonic Condensate in Quantum Hall Bilayers, *Phys. Rev. Lett.* **104**, 116802 (2010).
- [52] T. Hyart and B. Rosenow, Quantitative description of Josephson-like tunneling in $\nu_T = 1$ quantum Hall bilayers, *Phys. Rev. B* **83**, 155315 (2011).
- [53] A. D. K. Finck, J. P. Eisenstein, L. N. Pfeiffer, and K. W. West, Exciton Transport and Andreev Reflection in a Bilayer Quantum Hall System, *Phys. Rev. Lett.* **106**, 236807 (2011).
- [54] X. Huang, W. Dietsche, M. Hauser, and K. von Klitzing, Coupling of Josephson Currents in Quantum Hall Bilayers, *Phys. Rev. Lett.* **109**, 156802 (2012).
- [55] A. Perali, D. Neilson, and A. R. Hamilton, High-Temperature Superfluidity in Double-Bilayer Graphene, *Phys. Rev. Lett.* **110**, 146803 (2013).
- [56] G. W. Burg, N. Prasad, K. Kim, T. Taniguchi, K. Watanabe, A. H. MacDonald, L. F. Register, and E. Tutuc, Strongly Enhanced Tunneling at Total Charge Neutrality in Double-Bilayer Graphene-WSe₂ Heterostructures, *Phys. Rev. Lett.* **120**, 177702 (2018).
- [57] D. K. Efimkin, G. W. Burg, E. Tutuc, and A. H. MacDonald, Tunneling and fluctuating electron-hole Cooper pairs in double bilayer graphene, *Phys. Rev. B* **101**, 035413 (2020).
- [58] T. Paul, V. Fernández Becerra, and T. Hyart, Interplay of quantum spin Hall effect and spontaneous time-reversal symmetry breaking in electron-hole bilayers. II. Zero-field topological superconductivity, *Phys. Rev. B* **106**, 235421 (2022).
- [59] C. W. Groth, M. Wimmer, A. R. Akhmerov, J. Tworzydło, and C. W. J. Beenakker, Theory of the Topological Anderson Insulator, *Phys. Rev. Lett.* **103**, 196805 (2009).
- [60] D. I. Pikulin, T. Hyart, S. Mi, J. Tworzydło, M. Wimmer, and C. W. J. Beenakker, Disorder and magnetic-field-induced breakdown of helical edge conduction in an inverted electron-hole bilayer, *Phys. Rev. B* **89**, 161403(R) (2014).